EUROPEAN ORGANIZATION FOR NUCLEAR RESEARCH

PH 1/COM-71/2
7th January 1971

PHYSICS I

ELECTRONICS EXPERIMENTS COMMITTEE

Proposal for a Ξ^* experiment in the Omega Spectrometer

by

P. Astbury (Imperial College, London)
M. Barnett (I.C.L.)
D. Binnie (I.C.L.)
L. Camilleri (I.C.L.)
A. Duane (I.C.L.)
J. Gallivan (I.C.L.)
D. Garbutt (I.C.L.)
J. Jafar (I.C.L.)
W.G. Jones (I.C.L.)
J.G. Lee (I.C.L.)
M. Letheren (I.C.L.)
G. McEwen (Southampton)
I. Siotis (I.C.L.)
D. Websdale (CERN)
J.A. Wilson (I.C.L.)

INTRODUCTION

"The situation concerning the excited Ξ-states is very unpleasant. Since every octet and every decuplet requires an $I = \frac{1}{2}$ Ξ-state, we could get a vague impression of the expected Ξ-spectrum by combining the observed N and Δ states on the same plot. The predicted states should probably lie 250-400 MeV above the corresponding non-strange resonances ...." (Harari, Vienna 1968).

In the summary by the Particle Data Group (Ref. 1) only 3 Ξ states (1530, 1820 and 1930) are listed, despite relaxed selection criteria due to meagre statistics. The statistics are low because the cross-sections are no greater than a few microbarns and so far - 8 years after the introduction of RF-separated beams - the largest bubble chamber exposure has reached only 30 events/μb. The subject appears suitable for an Ω-experiment. On the one hand a trigger selecting incident K^- and recoil K^+ will yield an $S = -2$ state; on the other, the large angular acceptance and high momentum resolution of the Ω can be exploited to disentangle the complicated mixture of final states.

Arrangement of apparatus

Our design is at present based on spark chamber arrangement 2 with small chambers at the sides of the target with their plates parallel to the beam, Fig. 1. Five GeV/c K^- from the enriched beam (No. 3 of the beam subcommittee report, CERN 70-29) will be selected by Cerenkov counter. Most of the Ξ^* production cross section from the reaction $K^- + p \rightarrow \Xi^{*-} + K^+$ is expected to be in the backward peak associated with baryon exchange so that the K^+'s tend to come out of the target at large angles and with low momenta. Fig. 2 shows Ξ^* mass contours of θ_{K^+} as a function of both p_{K^+} and u, where

$$u = (m_p - m_K)^2 - 2m_p T_{K^+}$$

If the differential cross section is expressed as

$$\frac{d\sigma}{du} = \text{const.}\ e^{b(u-u_o)}$$

then from other hyperon exchange reactions we expect $b \sim 4\ (\text{GeV/c})^{-2}$.

Fig. 3 shows the momentum spectrum of the K^+ for different values of b, i.e.

$$\frac{d\sigma}{dP_{K^+}} = \frac{d\sigma}{du} \cdot \frac{du}{dP_{K^+}}$$

together with the momenta corresponding to the K^+ range in 2 cm of liquid hydrogen and in 100 gm cm^{-2} of copper. Bubble chamber results indicate that 2-body or quasi- 2-body interactions are generally associated with low momentum transfers; moreover, peripherally produced Ξ^* will be projected forwards into the main spark chambers where their secondary products can be accurately measured. The arrangement of the K^+ detectors will therefore be designed to select preferentially low momentum transfers, i.e. K^+ momenta less than 600 MeV/c.

In Fig. 4 we show a counter configuration compatible with spark chamber arrangement 2. There are three vertical counter arrays (V_1 V_2 V_3) and two horizontal arrays (H_1 H_2) mounted below the small spark chambers. The vertical counter V3 shown there can be relatively small because for Ξ^* mass $\leqslant 2.2$ GeV/c^2 the K^+ trajectories converge forwards into it. Figs. 5 & 6 are schematical layouts of the standard spark chambers together with the counters and two small additional chambers specific to our experiment.

K^+ Detectors

Each of the five counter arrays will consist of a sandwich of 9 scintillators interspersed with 8 copper plates. The counter V2 will contain 33 gm cm^{-2} of copper; the remaining counters will each contain 100 gm cm^{-2}. All counters will be supported on a trolley as shown in Fig. 7. The counter V3 has its own independent rails and its position can be adjusted during the experiment.

The position of the counter arrays was chosen by orbit tracing and by computer analysis of representative K^+-trajectories. With the aid of our Monte Carlo programme, SPRUCE, we tested and made minor modifications to the arrangement. The first four Monte Carlo events obtained for $m_{\Xi^*} = 1.8$ GeV/c^2 are illustrated in Fig. 8.

We show the K^+-stopping efficiency as functions of the slope b, Fig. 9 and the Ξ^*-mass, Fig. 10. Absorption in the hydrogen target, decay in flight and range in the counters have been included in evaluating this efficiency, but it represents only the stopping efficiency for K^+ and does not include the efficiency for the detection of the K^+-decay products.

For a Ξ^* mass of 1.8 GeV/c^2, V3 accounts for about 1/3 of the trigger rate, V1 and V2 together for rather more than 1/3 and the horizontal counters for the remainder. For a mass of 2.4 GeV/c^2, V1 accounts for 3/4 of the total and most of the remainder goes to V3. We give as an example in Fig. 11 a profile of K^+ intercepts with the plane containing V3 for $m_{\Xi^*} = 2.2$ GeV/c^2. This shows the focussing effect of the magnetic field; for lower masses this distribution is shifted further away from the beam and for higher masses towards the beam. This explains the falloff in efficiency with increasing mass as shown in Fig. 10. (V3 has a section, centred on the beamline, of radius 30 cm cut away to permit the Ξ^*-decay secondaries to enter the main chambers).

A sketch of a typical counter array is shown in Fig. 12. We have investigated the timing properties of a counter consisting of a small scintillator (NE 102A) mounted at the end of a 2 m light guide and viewed by a 56 AVP tube. The coincidence resolving time was 1.4 ns (FWHM) for 40 photoelectrons. The replacement of the 56 AVP by a high quantum efficiency tube (RCA 8575 has 31 %) is being investigated and could well improve the timing resolution as well as the dE/dx measurements. Tests have also shown that, by using passive pulse shaping elements at the phototube output, it is possible to obtain a 5 ns output pulse from a 56 AVP when a light diode is pulsed at the end of a 2 m light guide. Therefore, it appears reasonable to expect a scintillation counter to resolve two distinct particles separated by a time interval of about 7 ns. Further tests are being made but for the present it is assumed that a scintillation counter could clearly resolve two consecutive particles when the separation time is $\gtrsim$ 10 ns.

The slow recoil K^+ is stopped by a copper absorber plate and may be identified by the appearance of a delayed coincidence signal, from one of its charged products, in either one of the two scintillation counters adjacent to this absorber. Adjacent counters can be precisely timed relative to each other.

The triggering electronics may be divided into two logically distinct systems (F and B). System F will identify K^+ decay products emitted into the forward hemisphere (relative to the K^+ direction) within a gate width of 25 ns generated 6 ns after the prompt K^+ signal. These are called F triggers. On the other hand, system B will identify K^+ decay products emitted in the backward hemisphere and occuring inside the same gate but now delayed by 10 ns relative to the prompt K^+ pulse. The trigger F + B will include the $\mu^+ \nu$ and $\pi^+ \pi^0$ decay modes with branching ratios 63.8 % and 20.9 % respectively. Using the delays and the gate width indicated, 62 % of the forward and 44 % of the backward decaying K^+ will remain and, of these, 87 % will decay within the 25 ns gate. The detection efficiency for the K^+ decay is therefore estimated to be : $(0.62 + 0.44) \times 0.5 \times 0.87 \times (.64 + .21) = 0.39$.

Additional information that will be stored and monitored on-line will include relative timing and dE/dx measurements for the counter array that supplied the K^+ trigger. The K^+ range can be extracted from the array status word.

Yields and triggering rates

The following parameters are used in our yield calculations :

1) K^+ stopping efficiency, 0.4
2) K^+ decay detection efficiency, 0.39 } ϵ
3) Liquid hydrogen target length L, 40 cm
4) Liquid hydrogen density ρ , .07 gm cm^{-3}
5) K^- intensity N', 2. x 10^4 per PS burst (see NP Internal Report, 70-29)

then

$$\#\,\text{events}/\mu b/\text{burst} = N_0 \sigma \epsilon \; L.N'\rho = (6 \times 10^{23}) \times (10^{-30}) \times .16 \times 40. \times (2 \times 10^4) \times .07$$

$$= 5.2 \times 10^{-3}\ \text{events}/\mu b/\text{burst}.$$

Assuming a 20 hour PS day we get about 2000 events per microbarn for a 14 day PS period. In the present state of knowledge extrapolation from this figure to estimate the number of Ξ^*'s we can expect to obtain can be little better than speculation. We can only say that the cross sections for the peripherally produced Ξ^* (1820) and Ξ^* (2030) have been quoted as $\approx 3\,\mu b$ (ref. 4).

The figures that we have given above for the efficiency have been estimated from the available data. The major uncertainty is in the beam performance. We realise that it may not be possible to achieve adequate separation at 5.0 GeV/c. We would like to run at this momentum because it gives a range of Ξ^*-masses extending up to a phase space limit of 2.7 GeV/c^2. However, a beam momentum above 4.0 GeV/c still gives an interesting range of Ξ^*-masses up to 2.5 GeV/c^2.

It is difficult to predict the triggering background. No single proton and only 2 % of single pions stopping in the counters can simulate a K^+. We expect the triggering background to be due to such stopping particles accompanied by a delayed particle which spiralled in the magnetic field. This background, if troublesome, can be reduced by tightening the correlation between the layer in which the K^+ is thought to stop and the layers in which delayed decay pulses are seen. Accidental coincidences, due to high singles rates in the scintillators (background in the West Hall) can also be controlled by such adjustments. The on-line filtering cannot be very sophisticated. However the extensive information recorded on magnetic tape can subsequently be analysed to limit the number of measurements required on the HPD.

Kinematic Analysis and Identification of the Final State

In order to measure the branching ratios of the various Ξ^*'s it will be necessary to identify as many as possible of the final states in which the Ξ^* is produced. SU (3) calculations for some predicted Ξ^* states are given in Table 1 (from reference 5). The Ξ^* mass resolution is also dependent on the ability to identify the final state. Invariant mass gives a better mass resolution than the missing mass and the kinematic constraints at decay and production vertices can be used to improve significantly on this resolution.

Events will be selected in which the momentum of the particle entering the K^+ detector is consistent with the range and dE/dx measurement for K^+ and inconsistent with π or proton.

Certain restrictions are thus imposed on the final state. The system recoiling against the K^+ must have quantum numbers ($B = 1$, $Q = -1$, $S = -2$). Within this restriction many final states can be produced involving 'Ξ^*' decays into (nucleon, $\bar{K}\bar{K}$), ($\Sigma \bar{K}$, $\Lambda \bar{K}$), ($\Xi \pi$) and ($\Omega^- \bar{K}$) systems.

The next stage in the analysis will be to reconstruct and identify a V^0 decay. Table II contains a list of the final states satisfying the defined quantum number condition and specifies the V^0 decay to be identified. The corresponding topologies listed in this table are illustrated in figure 13. We define topology such that additional charged pions (and in the 4-C topologies, a neutral pion) can be included at the production vertex.

From our experience with the CERN-ETH-IC spark chambers we know that the direction of a neutral decay can be reconstructed with a precision ~ 1 mrad even when the vertex is not seen. The mean decay length of the Ξ^0 is 7 cm per GeV/c and of the Ξ^- it is 3.8 cm per GeV/c so the decay in topologies involving Ξ decays will originate from a point typically 20-25 cm from the production vertex ; its angular separation will be ~ 35 mrads.

Already it will be possible to separate the list of final states into certain categories :

i) a Λ coming from the production vertex can only result from $(\Lambda\bar{K})$ and $(\Sigma^0\bar{K})$ systems.

ii) a Λ which does not come from the production vertex identifies the $(\Xi\pi)$ systems (or production of Ω^-)

iii) a K^0_s decay, coming from the production vertex indicates the (nucleon $\bar{K}\bar{K}$) and $(\Sigma^\pm\bar{K})$ systems.

To determine the capabilities of the proposed set-up for resolving these final states and to assess the precision which is required from the K^+ momentum measurements we have made a Monte Carlo study. We have generated a sample of events of the type

$$\begin{array}{llll} K^- + p \to K^+ + \Xi^{*-}(1800) & & & P_{K^-} = 5\ \text{GeV}/c \\ & \searrow \Lambda K^- & & \\ & & \searrow p\pi^- & \end{array}$$

and $$K^- + p \rightarrow K^+ + \Xi^{*-}(1800)$$
$$\searrow \Xi^0 \pi^-$$
$$\searrow \Lambda \pi^0$$
$$\searrow p \pi^-$$

We then 'adjusted' the charged track parameters by adding perturbations corresponding to measurement errors and multiple scattering. These events were then passed through GRIND (the kinematic hypothesis testing programme) and we tried to identify these events with various hypotheses as listed below.

First the V^0 was tested with the hypotheses

$$\begin{array}{lcccc} K^0_s & \rightarrow & \pi^+ & + & \pi^- \\ \Lambda & \rightarrow & p & + & \pi^- \\ \bar{\Lambda} & \rightarrow & \pi^+ & + & \bar{p} \\ \gamma & \rightarrow & e^+ & + & e^- \end{array}$$

and then at the production vertex

$$\begin{array}{lcl} K^- + p & \rightarrow & \Lambda K^+ K^- \\ & & \Sigma^0 K^+ K^- \\ & & \Lambda K^+ K^- \pi^0 \\ & & \Lambda \pi^+ \pi^- \\ & & \Sigma^0 \pi^+ \pi^- \\ & & \Lambda \pi^+ \pi^- \pi^0 \end{array}$$

The last three hypotheses have been included here to assess the importance of the independent K^+ identification. The measurement errors used to 'adjust' the momenta of the charged particle trajectories are the same as those found in the CERN-ETH spark chamber photographs measured with the HPD; multiple scattering errors corresponding to the Omega radiation length of 70 meters were used. The K^+ measurement errors have however been treated independently and various values have been tried (spatial resolution σ_y ranging from 0.5 mm to 10 mm). The results of this preliminary analysis are given in Tables III → V.

In Table III the GRIND results from the 100 generated Λ's are shown. On the basis of a χ^2 cut of 1 % 84 of these Λ's were unambiguously identified. The Ξ^0 events were used to examine the performance of the system in identifying topology. We have not yet incorporated in our GRIND programme the possibility of testing the $\Xi^0 \to \Lambda \pi^0$ hypothesis (a decay vertex with no measured tracks) so we have studied the results of trying to fit events generated as Ξ^0's to the hypotheses of topology A, where the Λ originates from the production vertex. The results are given in Table IV for two different assumptions on the K^+ measurement precision. Only ~ 20 % of events fit topology A. Moreover the $\Lambda K^+ K^-$ hypothesis is virtually uncontaminated. As expected the angular precision on the direction of the reconstructed Λ is sufficient to exclude its origin at the production vertex except in the case of short Ξ decay lengths or forward-backward $\Xi \to \Lambda \pi$ decays.

The events generated as $\Lambda K^+ K^-$ are listed in Table V. We see that $\Lambda - \Sigma^0$ ambiguities are the main problem; after a $P(\chi^2) > 1$ % cut only 35-40 % of the ΛK^+K^- events can be unambiguously identified and this does not appear to depend critically on the K^+ measurement precision. We shall therefore be obliged to treat this ambiguity with statistical techniques similar to those used in bubble chambers. Figure 15, for example, is a plot of the fitted γ energy from the Σ^0 decay. Genuine Σ^0's of momentum about 3.3 GeV/c should have a very different spectrum with 85 % of γ energies higher than 75 MeV/c. Here again we see that the prior K^+ identification serves to eliminate the high cross section $\Lambda \pi^+ \pi^- \pi^0$ state.

The remaining final states involve a K^os decay from the production vertex. We have found in previous experiments that the identification of K^os decays (even if the apex is not seen) is not difficult. The problem of the Λ-K ambiguity is less serious for genuine $K^o_s \rightarrow \pi^+ \pi^-$ than for genuine $\Lambda \rightarrow p \pi^-$. The (nucleon $\bar{K}K$) systems provide 1-C and 4-C fits without problems but the ($\Sigma^\pm \bar{K}$) systems will be more difficult since the Σ decay will often not be seen in the chambers. $\Sigma^\pm$ decays however belong to unique (bar Ω^-) topologies. When $\Sigma^\pm$ decay is seen a 4-C production vertex fit can be made but if not the fit is 1-C and the K^+ momentum measurement is importan

As an example of the mass resolution we plot in figure 16 the invariant mass of events generated as Ξ^* (1800) $\rightarrow \Lambda K^-$. The upper figure shows the mass from the charged decay products; below are shown the same events analysed as a 4-C fit. Despite the large K^+ errors assumed (σ = 10 mm) the distribution is well centred and the width significantly reduced.

We have seen above that although we can resolve fairly satisfactorily most of the Ξ^* decay modes we shall be left with some ambiguities which must be carefully examined to minimise biases in measuring branching ratios and angular distributions. Most of the ambiguities will arise from short decay lengths, but the number of these can be estimated. Second order effects will bias the trigger efficiency - for example, $\Xi^- \pi^+ \pi^-$ will interfere more with V_3 triggers than will ΛK^-. Here and elsewhere we shall be greatly helped by having 5 independent decay detectors. And, as in bubble chamber experiments, the weights introduced to allow for detection efficiency can be checked by comparing for example $\Sigma^o K^-$ and $\Sigma^- K^o$.

Concluding remarks

If and when our proposal is accepted as a potential Ω experiment we will build a counter array with light guides as illustrated in figure 12 and test its efficiency for K^+ detection at the Rutherford laboratory or at CERN. When we are satisfied with its performance we will construct and test the remaining counter arrays. We hope then that we shall be able to test one or more of the counter arrays in the Ω magnet. We do not think that our counter V2 should disturb unduly any other user. If one or more other users were prepared to run with the chamber around the target restricted in depth to 125 cm we could also test counter arrays H_1 and H_2. The counter V_1 could be tested during runs with a fast forward trigger; we should like also to explore the possibility of using a fast proton trigger in parallel with our own K^+ trigger or at least to use the forward Cerenkov counter to increase our efficiency in Λ identification.

We can obtain useful data in an unseparated beam and although we would prefer to run at about 5 GeV/c we do not exclude other momenta. We have made a Monte Carlo trial of our detection efficiency for Ξ^* 1800 at 8 GeV/c. The stopping efficiency for V_2 alone is 9 %. For H_1 and H_2 it is 9 %, for V_1 6 % and for V_3 placed 60 cm from the beam line it is 11 %. We can moreover make valuable trials of K^+ detection from the reaction $\pi^- + p \rightarrow Y^{-*} + K^+$.

Despite the evident inconvenience of our counter V_3 we think that several other users should be able to make useful tests during a Ξ^* production run. Our provisional design ensures that our apparatus can be quickly rolled in and out of the magnet; we expect that after more detailed discussion with other users we shall be able to modify it in the interests of overall compatibility.

We hope that the two small chambers in front of the target, sketched in figure 5, could be made at CERN. Although the design that we have discussed here is based on the use of standard chambers flanking the target we could obtain greater precision in K^+ measurement by using special chambers which we could design and construct ourselves. We are glad to acknowledge the advice which we have received from Dr. Gildemeister concerning possible chambers and hope that we may continue in the future to profit from his guidance.

We should like to do some preliminary measurements with HPD Ω but 1/3 of the time on the Imperial College HPD is used for magnet spark chamber measurements; this should be adequate for the modest number of photographs that we expect to measure.

FIGURES

1. Spark Chamber arrangement 2.
2. P_{K^+} vs θ_{K^+}, kinematics for $K^- p \rightarrow \Xi^* K^+$
3. $d\sigma/dP_{K^+}$
4. Counter arrangment, plan view.
5. Complete apparatus, plan view
6. Complete apparatus, elevation
7. Chariot supporting counters
8. Sample trajectories $K^- + p \rightarrow \Xi^*(1800) + K^+$
9. K^+ stopping efficiency as a function of the slope, b.
10. K^+ stopping efficiency as a function of Ξ^* mass.
11. Y-Z profile of K^+ at V3
12. Sketch of counter module
13. Topologies satisfying $B = +1$, $Q = -1$, $S = -2$.
14. $P(X^2)$ for Monte Carlo generated Λ decays analysed as Λ and as K_s^0 decays.
15. γ-energy spectrum observed when Monte Carlo generated $\Lambda K^+ K^-$ events can be fitted as $\Sigma^0 K^+ K^-$.
16. Mass distribution of $\Xi^*_{1800} \rightarrow \Lambda K^-$

REFERENCES

1. H.Harari, page 205, 1968, Vienna Conf. Proc.
2. Particle Data Group, Phys. Letters 33B, 121 (1970).
3. Beam Subcommittee report (CERN NP 70-29).
4. J.Alitti et al. Phys.Rev.Letters 22 (1969)79 .
5. D.E.Plane et al. Nucl.Phys. B 22 (1970)93.

Table I

SU(3) Decay Rates (ref. 5)

Multiplet	PREDICTED			OBSERVED [(a)]		
	Mass (MeV)	Decay Mode	Partial width (MeV)	Mass (MeV	Total Width (MeV)	Comments
$7/2^+$ Decuplet	2160			-	-	
		$\Xi\pi$	21			No observed
		$\Sigma\bar{K}$	15			candidate
		$\Xi\eta$	3			
		$\Lambda\bar{K}$	26			
$5/2^-$ Octet	1950			1930	~110	
		$\Xi\pi$	70			$\Xi\pi$ large
		$\Sigma\bar{K}$	18			
		$\Xi\eta$	0			
		$\Lambda\bar{K}$	14			$\Lambda\bar{K}$ small
$5/2^+$ Octet	1985			2030	~ 50	
		$\Xi\pi$	0			$\Xi\pi$ small
		$\Sigma\bar{K}$	25			$\Sigma\bar{K}$ ~70%
		$\Xi\eta$	0			
		$\Lambda\bar{K}$	5			$\Lambda\bar{K}$ ~20%
$1/2^-$ Nonet	1825			1820	~30	
		$\Xi\pi$	62			$\Xi\pi$ ~10%
		$\Sigma\bar{K}$	17			
		$\Lambda\bar{K}$	80			$\Lambda\bar{K}$ ~30%
$3/2^-$ Nonet	1800			1820	~30	
		$\Xi\pi$	4			$\Xi\pi$ ~10%
		$\Sigma\bar{K}$	5			
		$\Lambda\bar{K}$	7			$\Lambda\bar{K}$ ~30%

Table II

$K^- + p \rightarrow K^+$		V^0 to be identified	Topology*
+ (nucleon $\bar{K}\bar{K}$)	$n K^- \bar{K}^0$	K^0_s	A
	$p \pi^- K^- \bar{K}^0$	K^0_s	A
$(\Lambda \bar{K})$	ΛK^-	Λ	A
	$\Lambda \pi^- \bar{K}^0$	Λ, K^0_s	A
	$\Lambda K^- \pi^0$	Λ	A
$(\Sigma \bar{K})$	$\Sigma^0 K^-$	Λ	A
	$\Sigma^0 \pi^- \bar{K}^0$	$\Lambda + K^0_s$	B
	$\Sigma^- \bar{K}^0$	K^0_s	C
	$\Sigma^- K^- \pi^+$		D
	$\Sigma^+ K^- \pi^-$		D
	$\Sigma^+ \bar{K}^0 \pi^- \pi^-$	K^0_s	C
$(\Xi \pi)$	$\Xi^- \pi^0$	Λ	E
	$\Xi^- \pi^+ \pi^-$	Λ	E
	$\Xi^0 \pi^-$	Λ	F
	$\Xi^0 \pi^- \pi^+ \pi^-$	Λ	F

* Non-decaying charged prongs at the production vertex are not considered as separate topologies

Table III

100 events generated

$$\begin{tikzcd}[column sep=small, row sep=small]
K^- + p \arrow[r] & \Xi^{*-}(1800) \arrow[dr] & + & K^+ \\
& & \Lambda \arrow[dr] & K^- \\
& & & p\pi^-
\end{tikzcd}$$

Results of fit to decay vertex :

(i)	Λ fit $P(\chi^2) > 1\%$	100
(ii)	Uniquely identified Λ's	84
(iii)	$\Lambda - K_s^0$ ambiguous	15
(iv)	$\Lambda - \gamma$ ambiguous	1

Table IV

100 events generated

$$\begin{tikzcd}[column sep=small, row sep=small]
K^- + p \arrow[r] & \Xi^{*-}(1800) \arrow[dr] & + & K^+ \\
& & \Xi^0 \arrow[dr] & \pi^- \\
& & & \Lambda\pi^0
\end{tikzcd}$$

	K^+ errors $\begin{matrix}\sigma_y \\ \sigma_z\end{matrix}$	·5 mm 1·5 mm	1 mm 3 mm
(i)	Events measurable ($\Delta p_{K^+} < p_{K^+}$)	94	89
(ii)	Events incompatible with K^+ and Λ originating at production vertex	76	63
(iii)	$\Lambda K^+ K^-$ fits $P(\chi^2) > 1\%$	1	1
(iv)	$\Sigma^0 K^+ K^-$ fits "	14	13
(v)	$\Lambda K^+ K^- \pi^0$ fits "	14	15
(vi)	$\Lambda \pi^+ \pi^- \pi^0$ fits "	30	2

Table V

100 events generated as

$$K^- + p \rightarrow \Xi^{*-}(1800) + K^+$$
$$\Xi^{*-} \rightarrow \Lambda K^-$$
$$\Lambda \rightarrow p\pi^-$$

K^+ measurement errors used

σ_y	·5 mm	1 mm	10 mm
σ_z	1·5 mm	3 mm	10 mm
Events measurable ($\Delta p_{K^+} < p_{K^+}$)	96	93	85
$\Lambda K^+ K^-$ fits $P(\chi^2) > 1\%$	96	92	85
$\Sigma^0 K^+ K^-$ fits $P(\chi^2) > 1\%$	61	54	55
$\Lambda K^+ K^-$ fits uniquely identified	35	39	30
$\Lambda K^+ K^- \pi^0$ fits	0	0	0
In addition there were:			
$\Lambda \pi^+ \pi^- \pi^0$ fits	39	44	37
$\Sigma^0 \pi^+ \pi^-$ fits	5	6	4

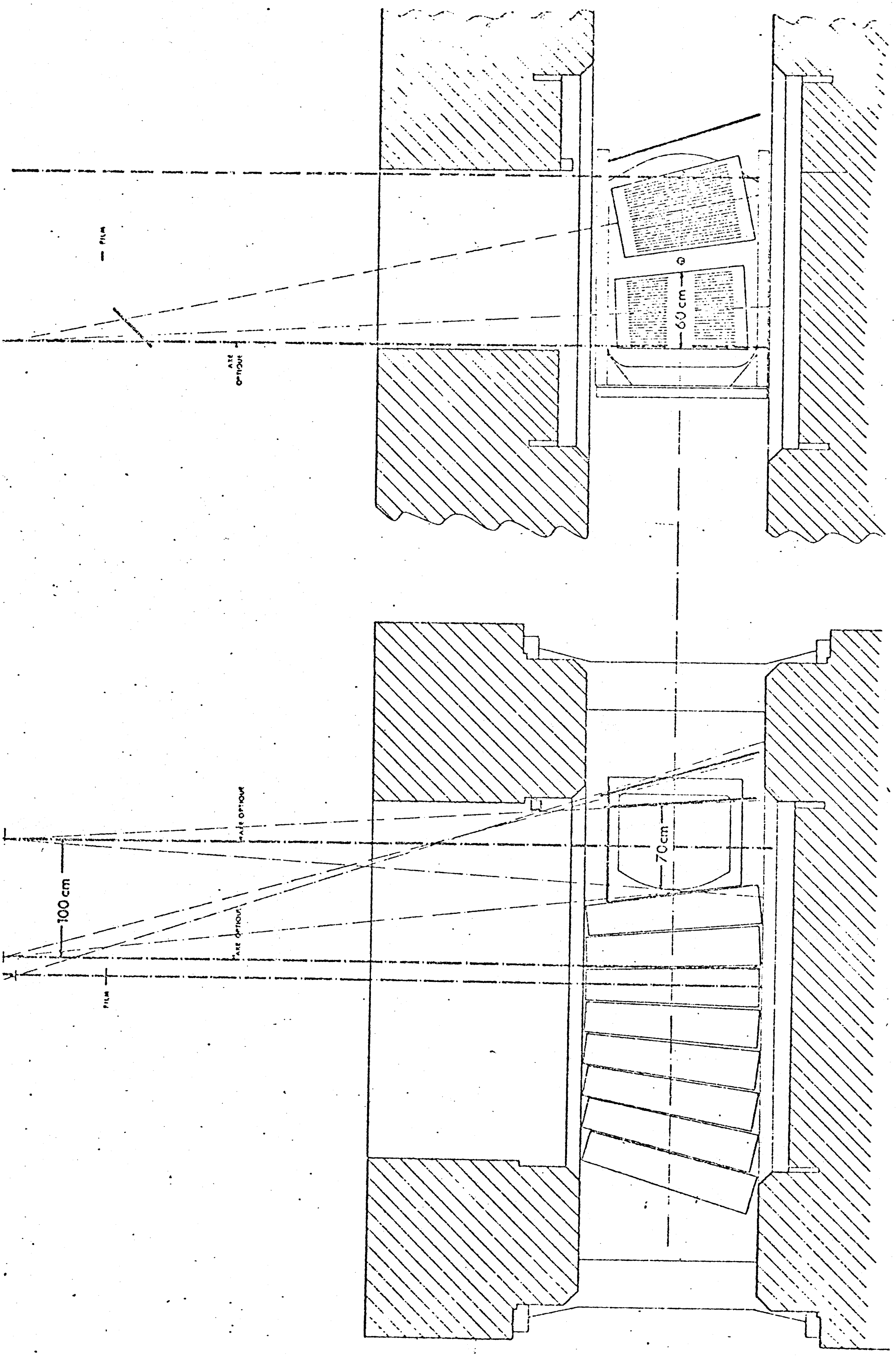
FILM
AXE OPTIQUE
60 cm
100 cm
AXE OPTIQUE
AXE OPTIQUE
FILM
70 cm

FIG. 1

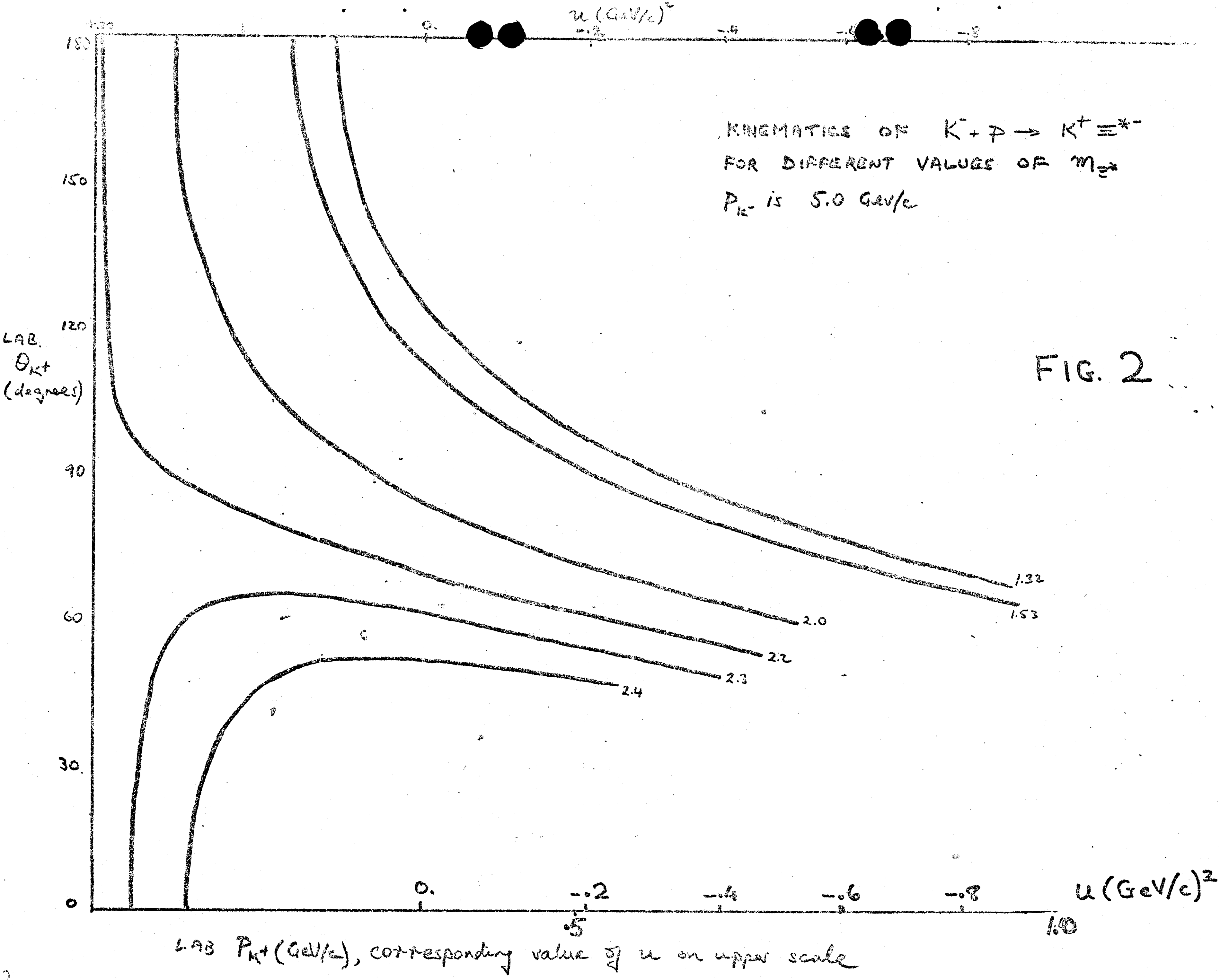

KINEMATICS OF $K^- + p \rightarrow K^+ \Xi^{*-}$
FOR DIFFERENT VALUES OF M_{Ξ^*}
P_{K^-} is 5.0 GeV/c

FIG. 2

K$^+$ MOMENTUM SPECTRUM FOR DIFFERENT SLOPES IN $\frac{d\sigma}{du}$.

FIG. 3

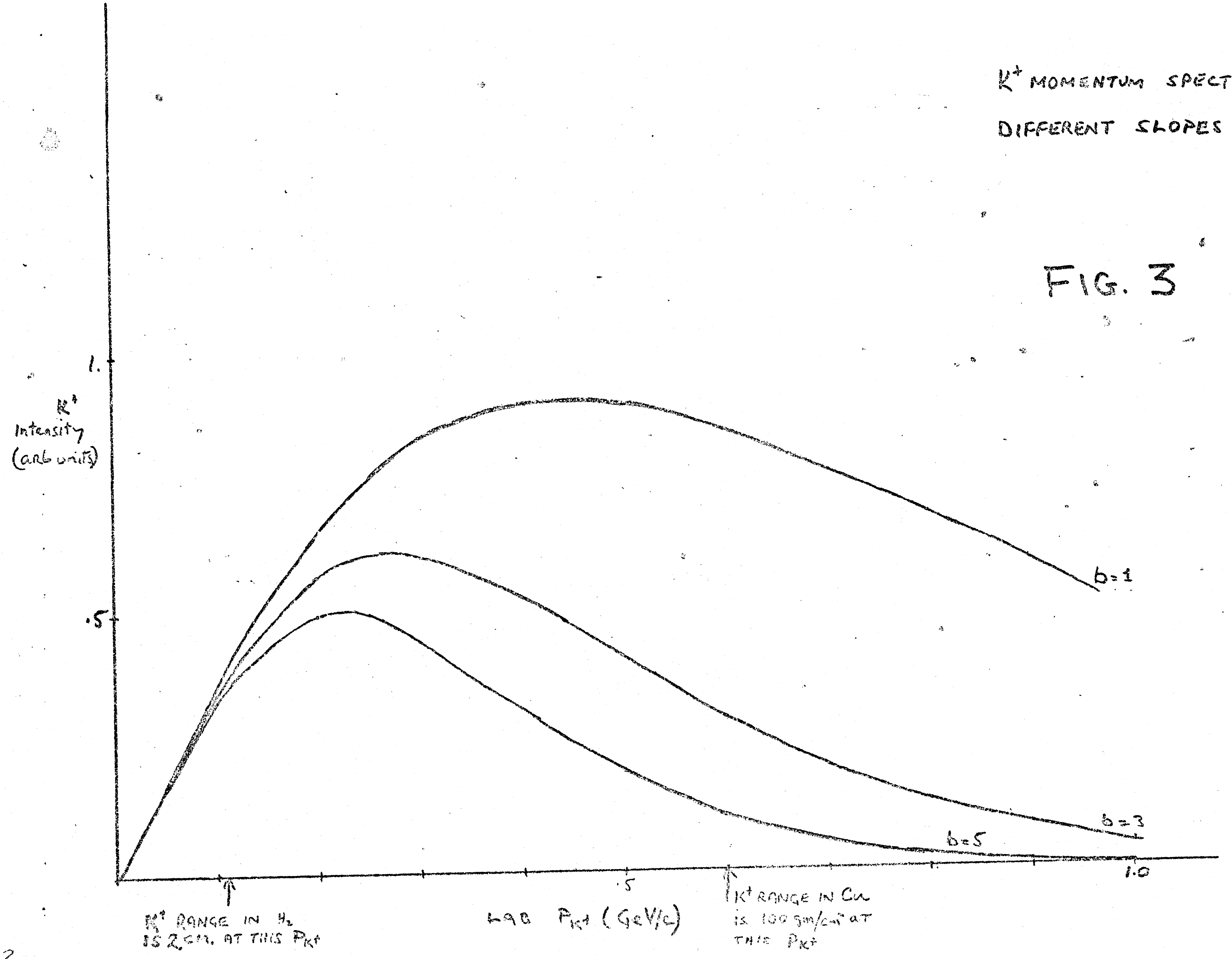

FIG. 4

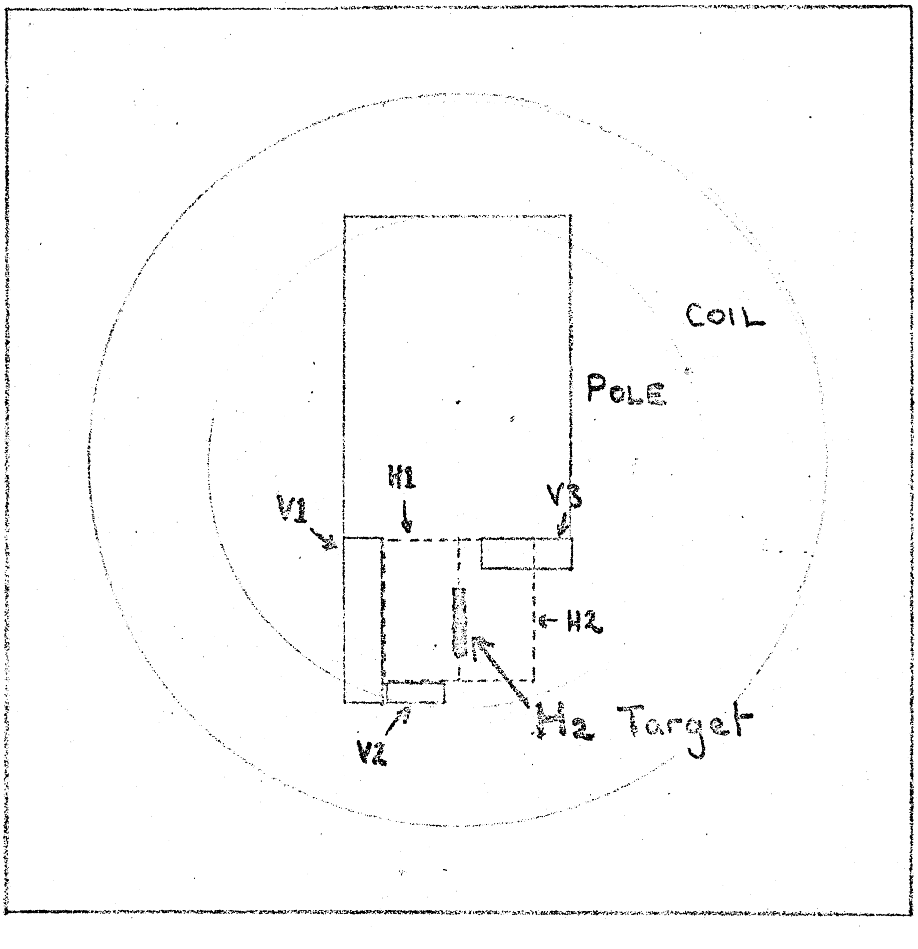

FIG. 5

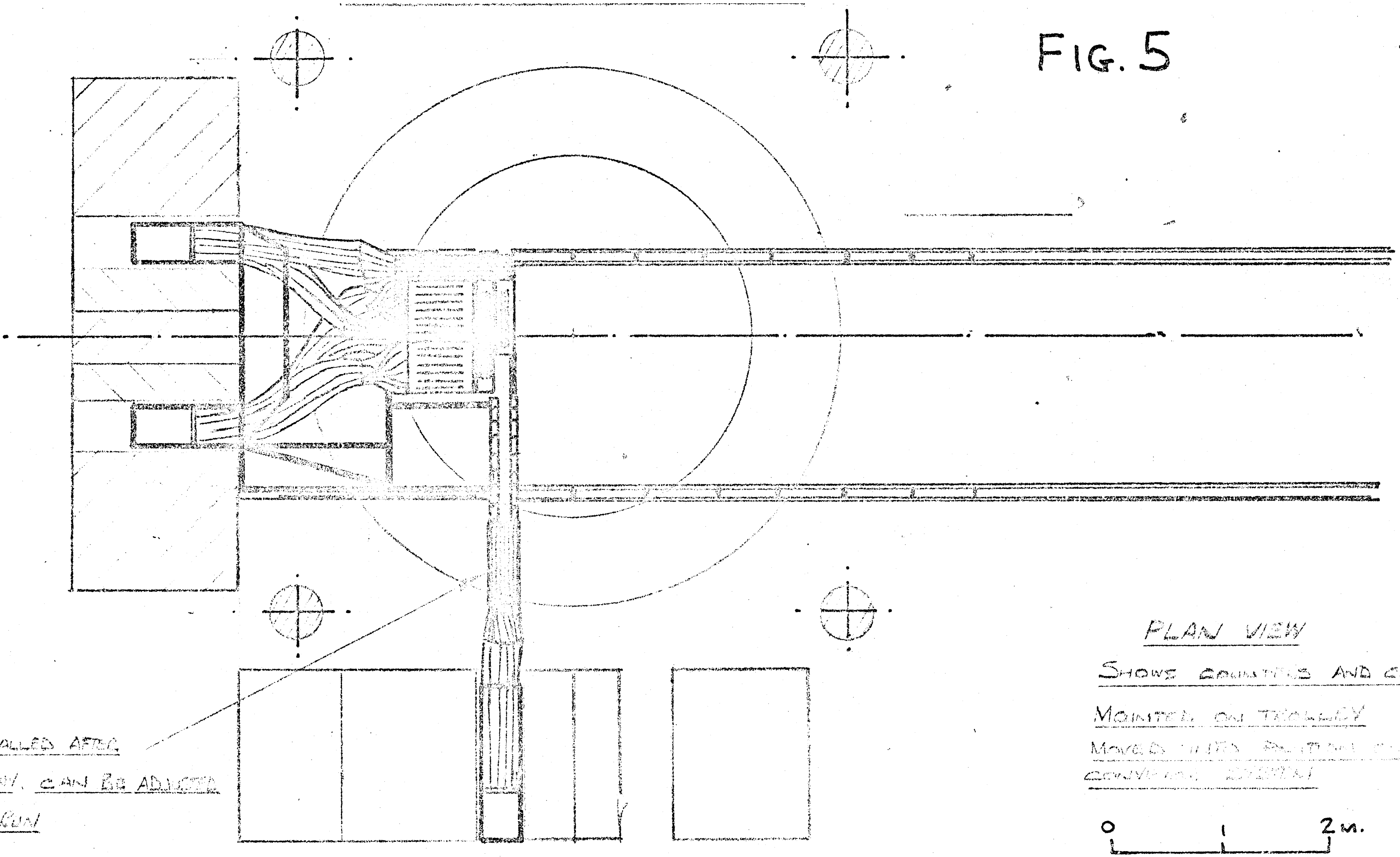

PLAN VIEW

SHOWS COUNTERS AND CHAMBERS
MOUNTED ON TROLLEY
MOVED INTO POSITION ON
CONVEYOR SYSTEM

0 1 2M.

SCALE.

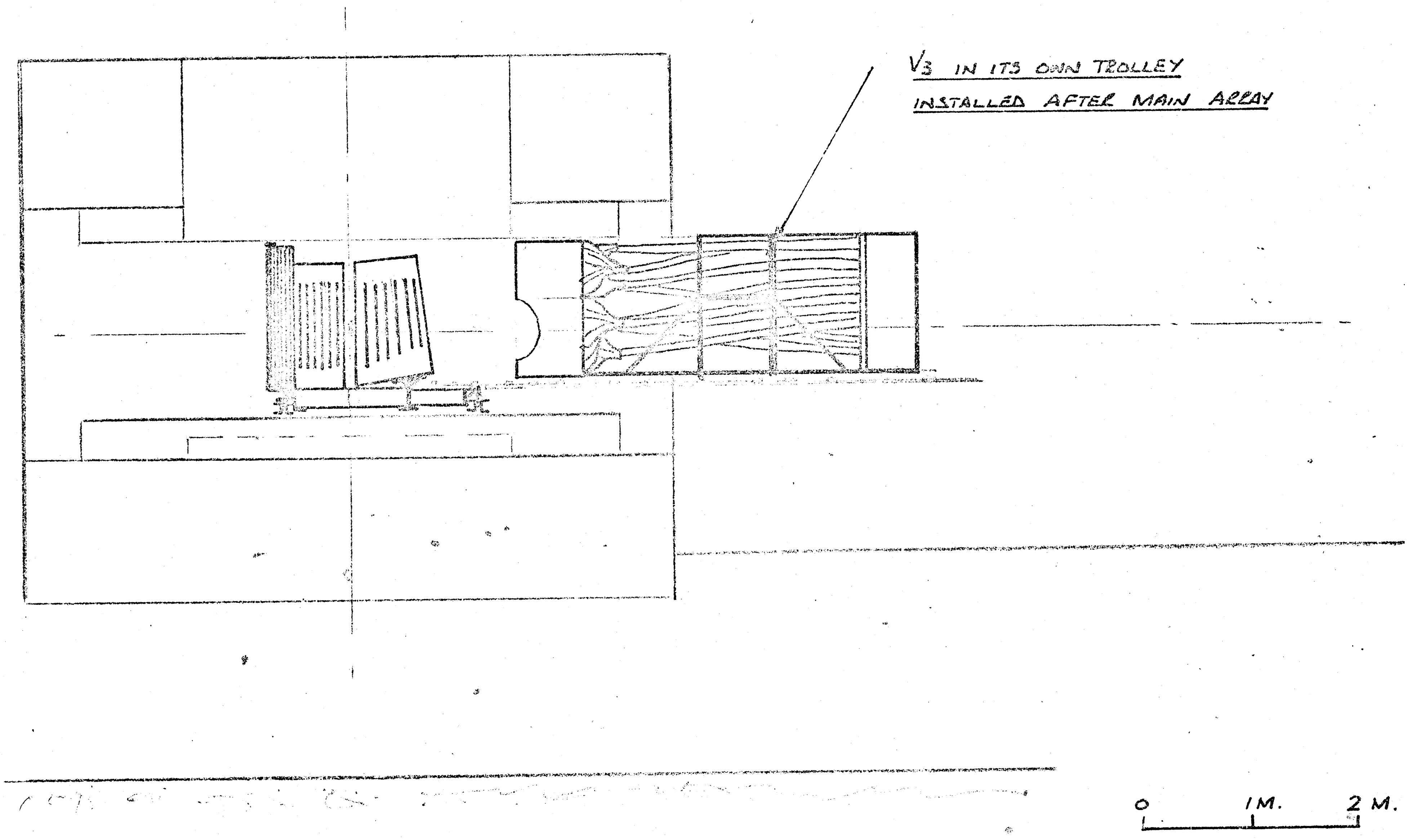

FIG. 6 END VIEW

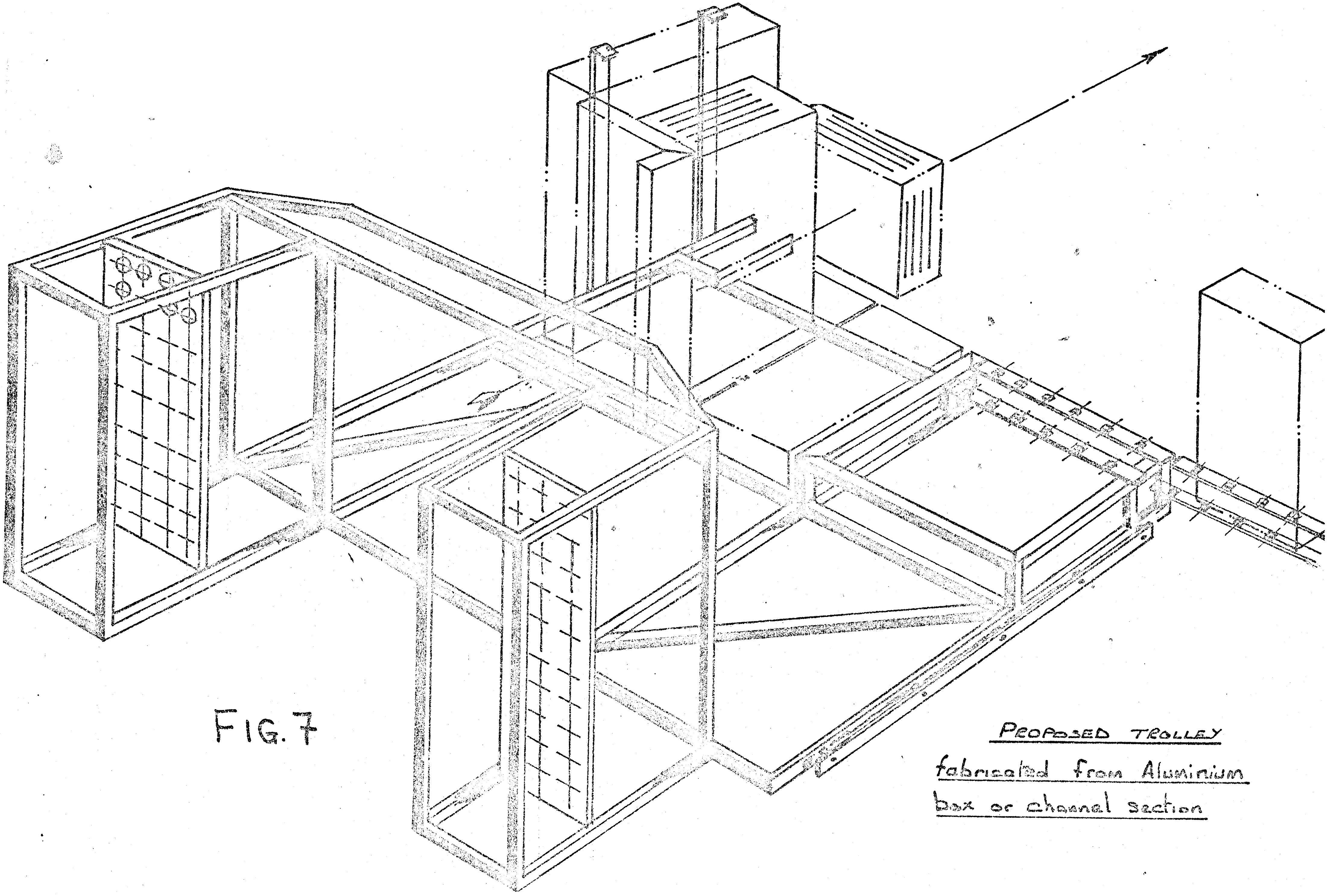

FIG. 7

PROPOSED TROLLEY

fabricated from Aluminium box or channel section

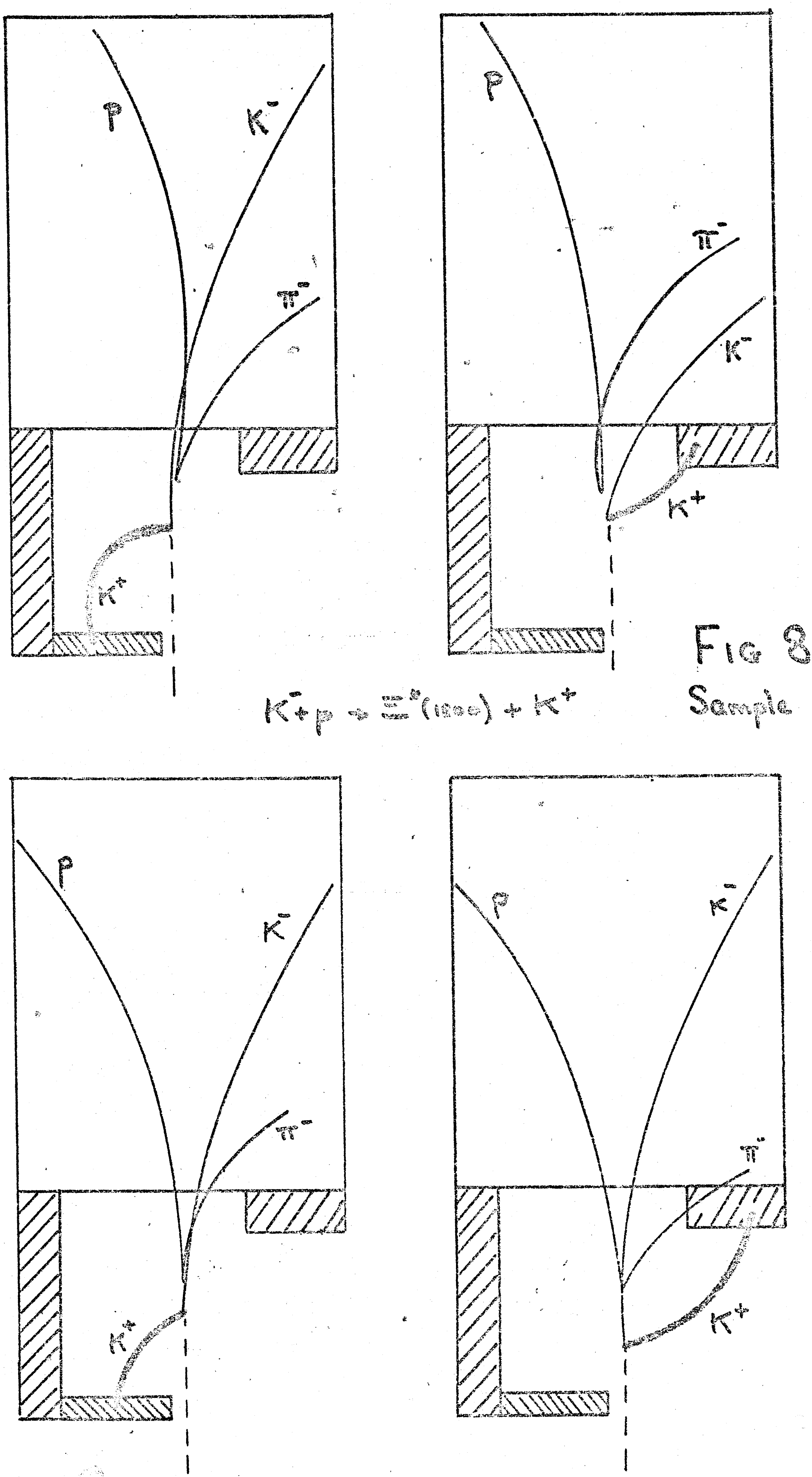

$K^- + p \to \Xi^0(1800) + K^+$

Fig 8
Sample trajectories

FIG 9

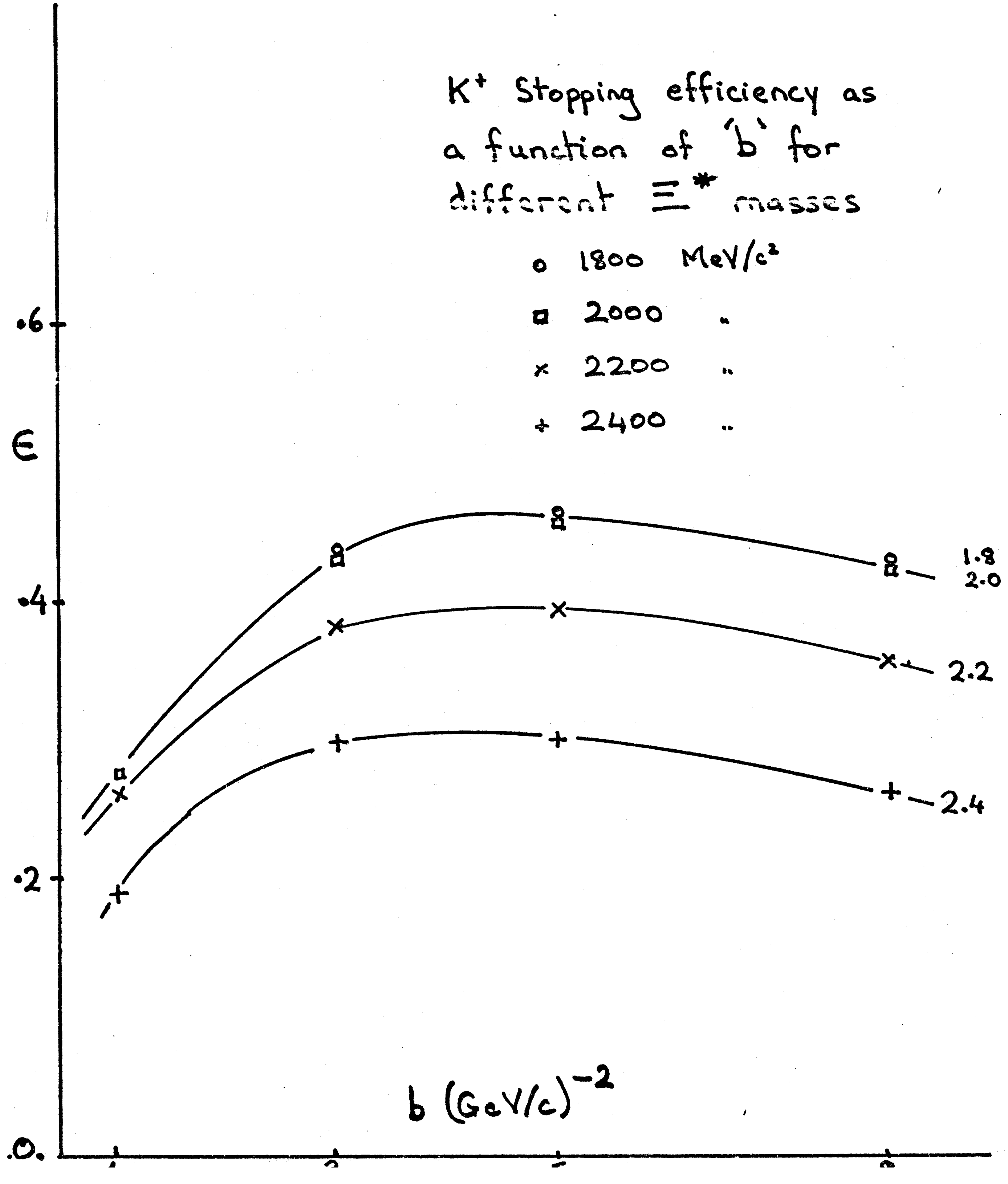
K⁺ Stopping efficiency as a function of 'b' for different Ξ* masses

FIG. 10

K^+ Stopping efficiency as a function of M_{Ξ^*} for different values of b

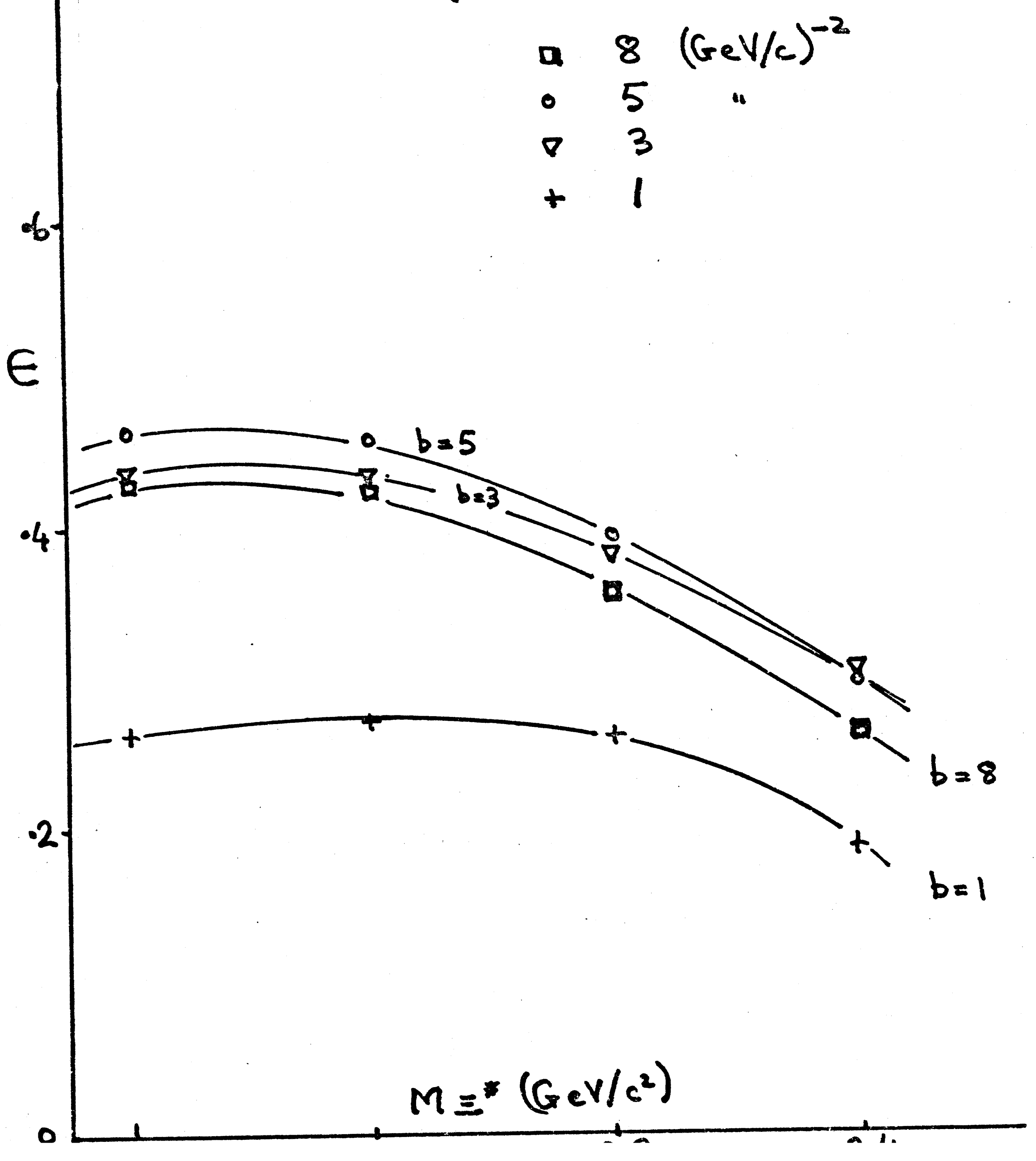

Fig. 11

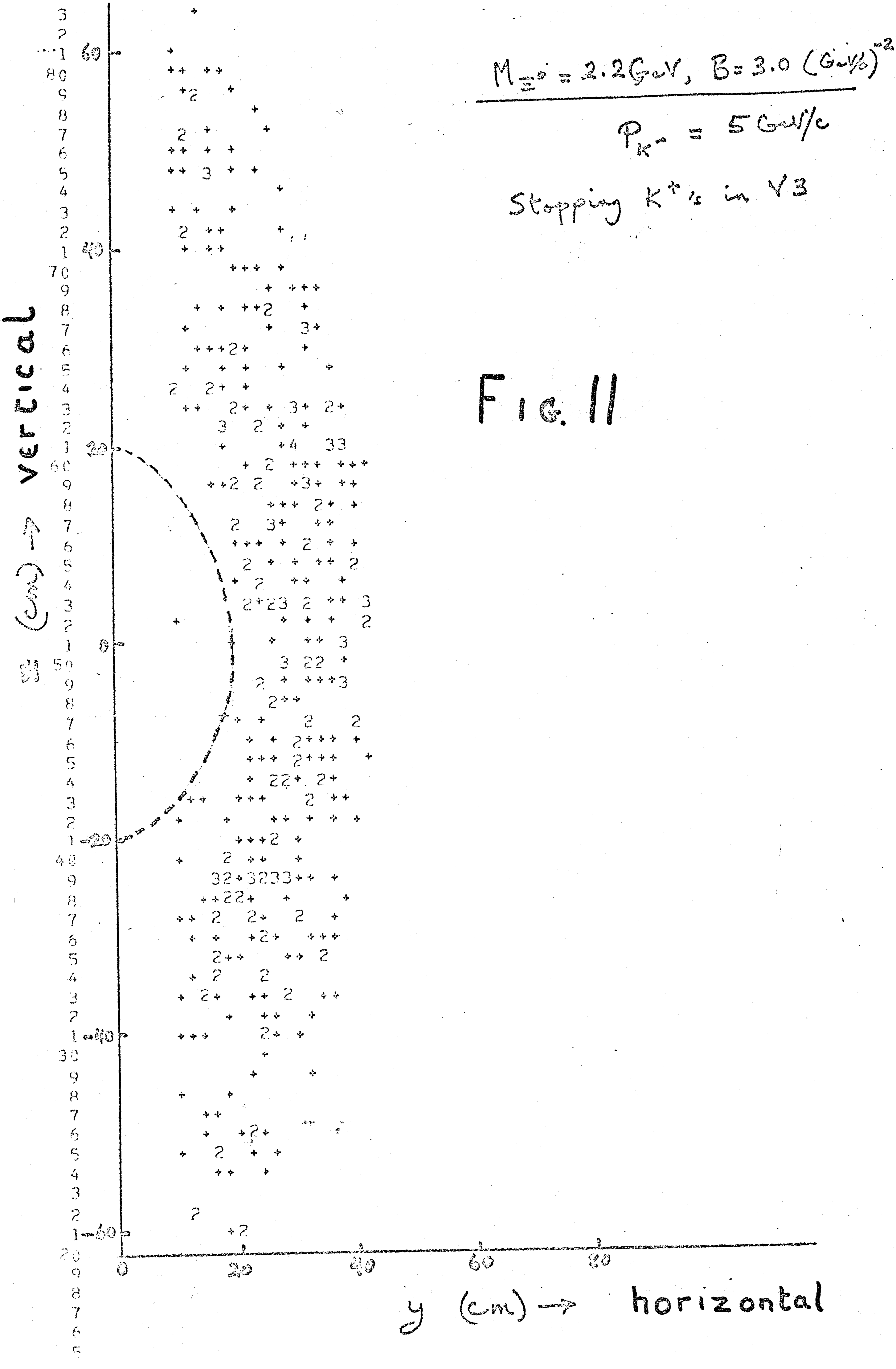

$M_{\Xi^0} = 2.2\,\mathrm{GeV}$, $B = 3.0\,(\mathrm{GeV}/c)^{-2}$

$P_{K^-} = 5\,\mathrm{GeV}/c$

Stopping K^+'s in V3

Fig. 12

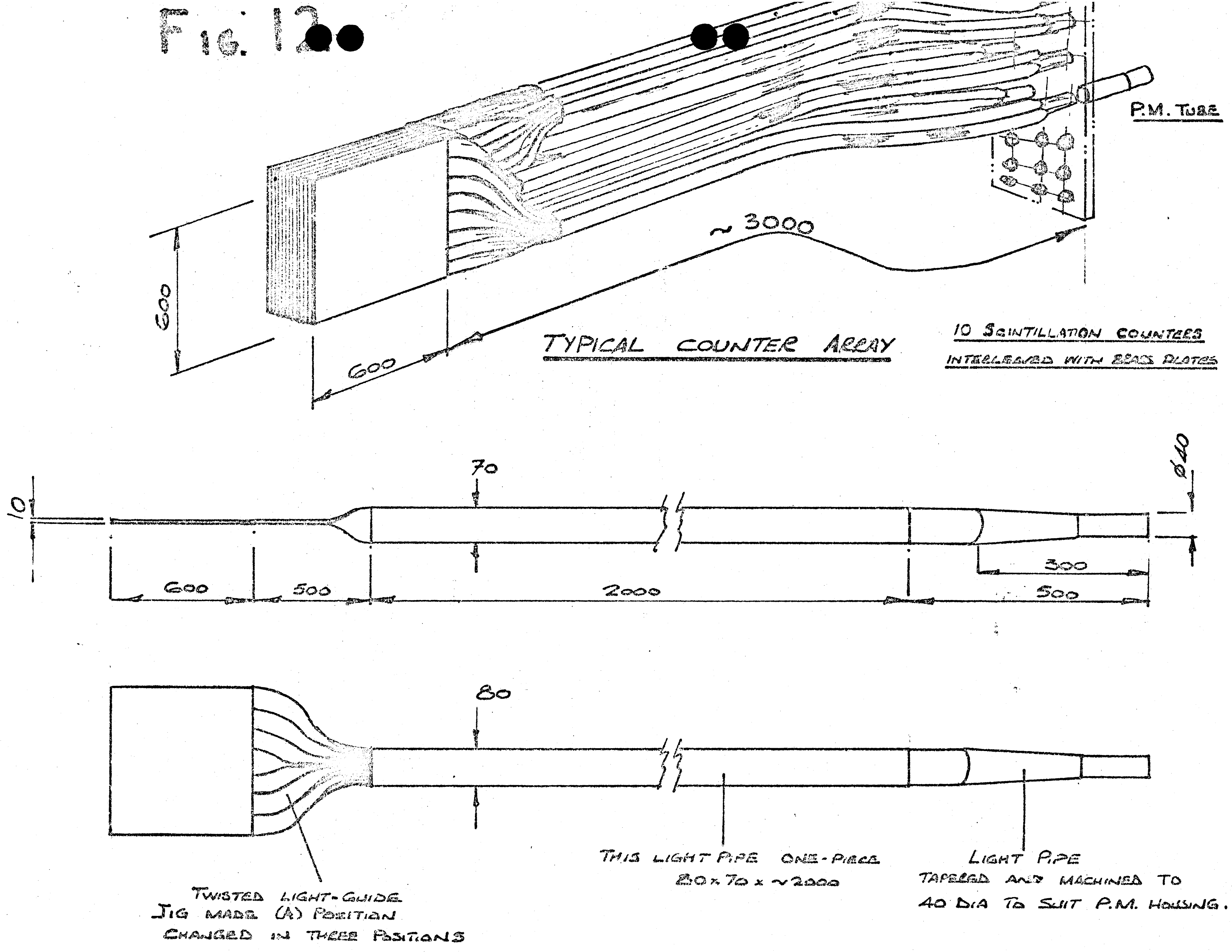
P.M. Tube
~ 3000
600
600
TYPICAL COUNTER ARRAY
10 Scintillation counters
interleaved with brass plates
70
10
⌀40
600
500
2000
300
500
80
This light pipe one-piece
80 × 70 × ~2000
Light pipe
tapered and machined to
40 dia to suit P.M. housing.
Twisted light-guide
Jig made (A) position
changed in three positions

FIG. 13. Topologies with $B = 1$
$Q = -1$
$S = -2$

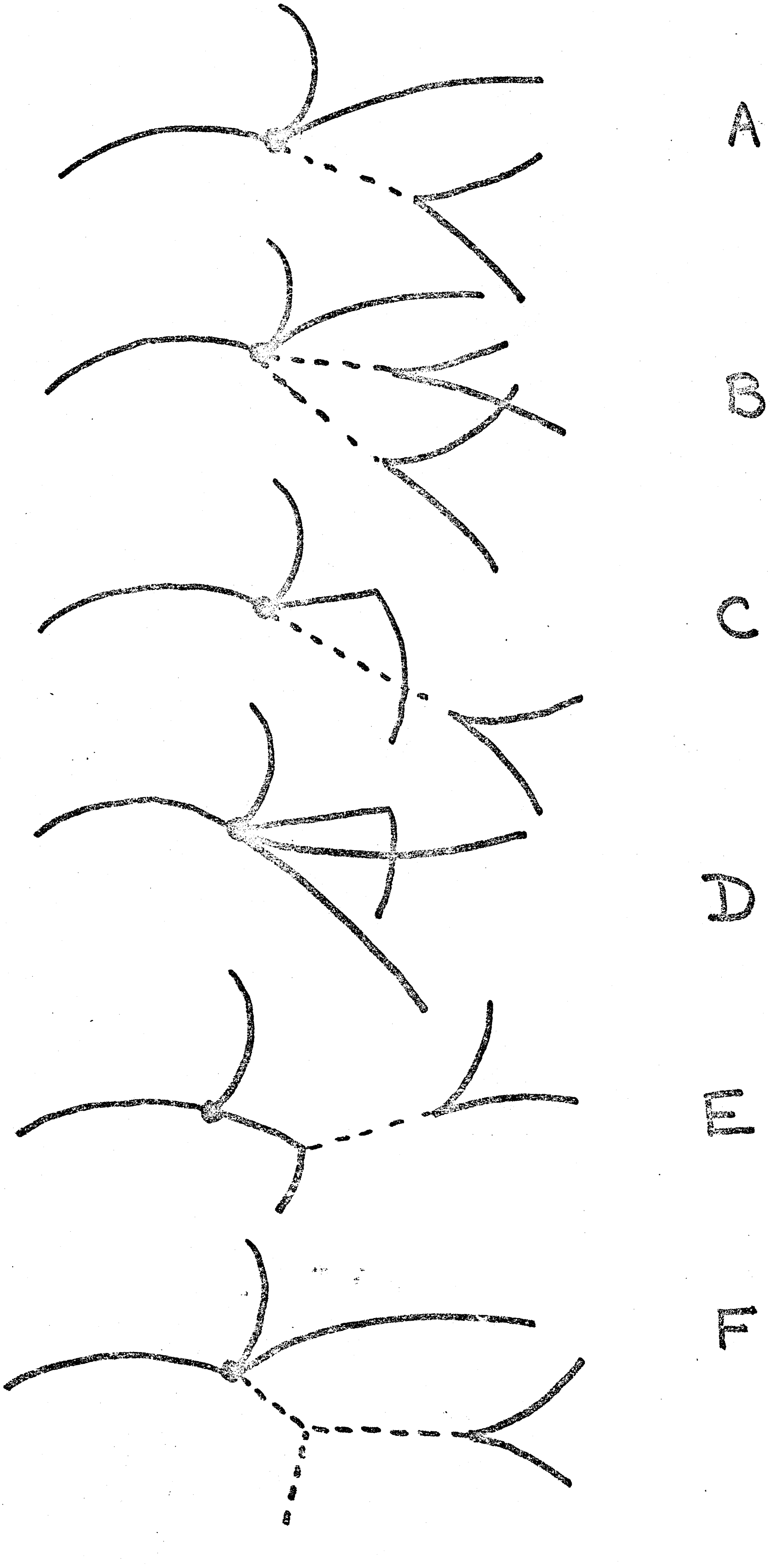

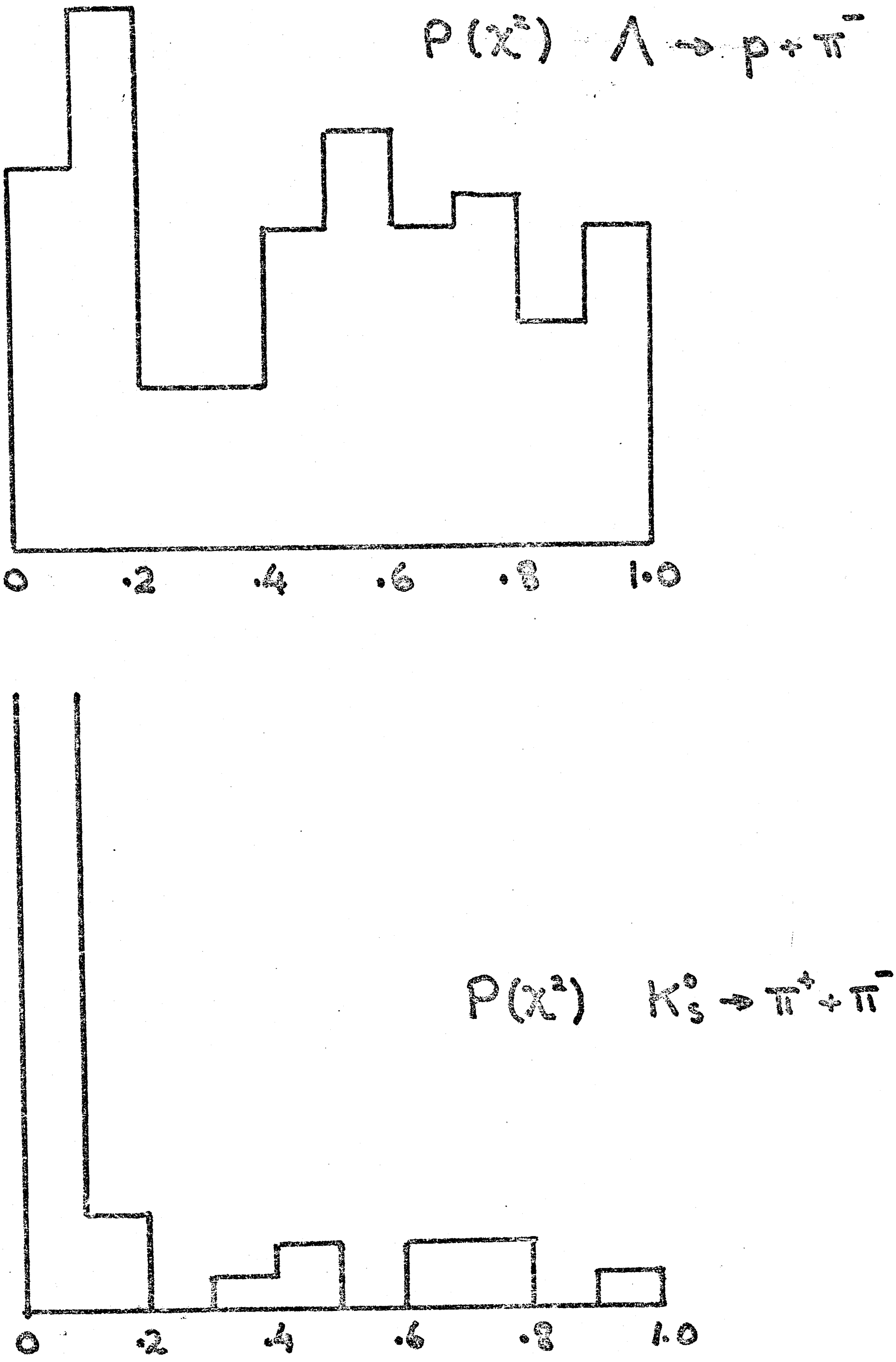
$P(\chi^2)$ $\Lambda \rightarrow p + \pi^-$
0
·2
·4
·6
·8
1·0
$P(\chi^2)$ $K_s^0 \rightarrow \pi^+ + \pi^-$
0
·2
·4
·6
·8
1·0

FIG. 14

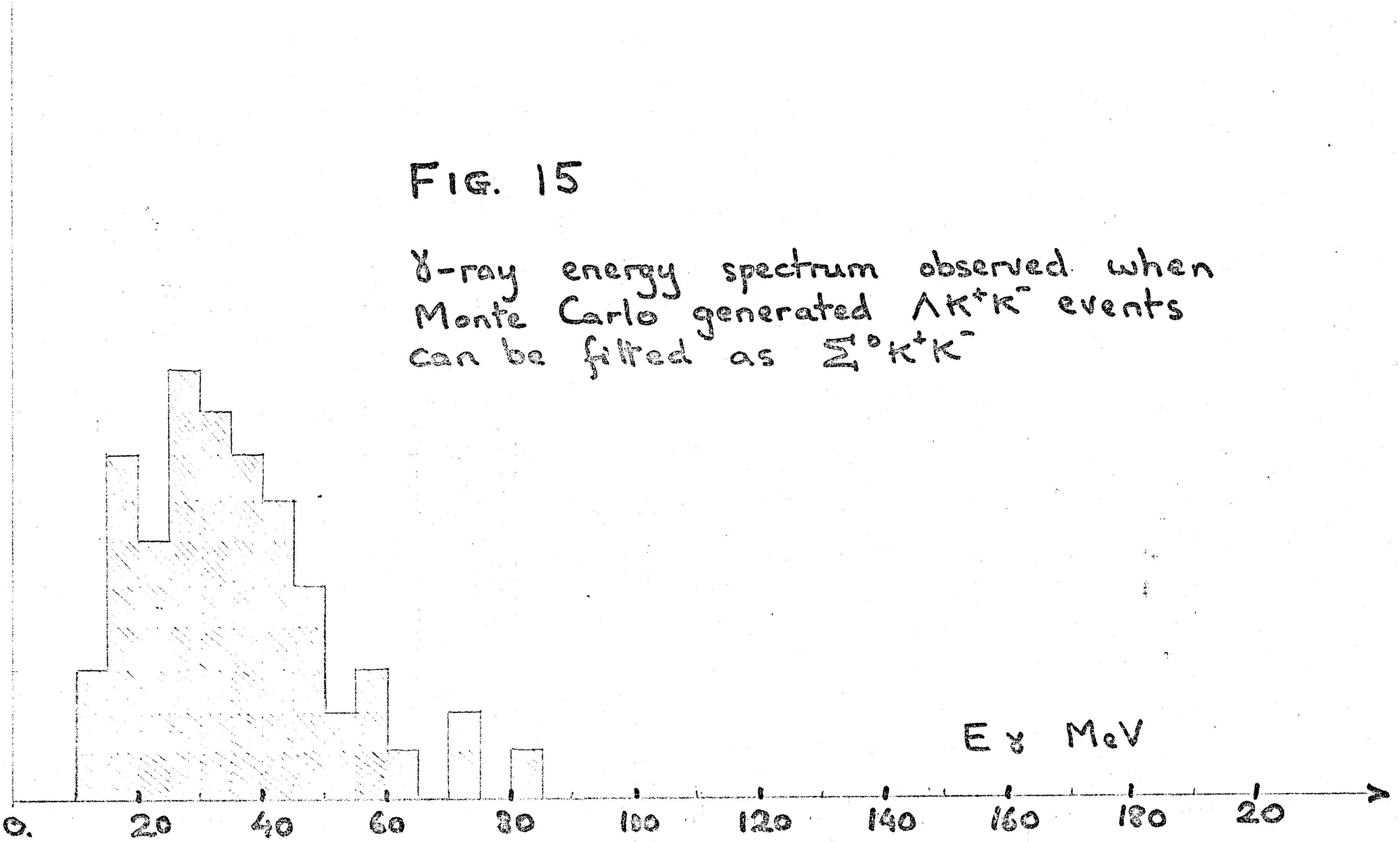

FIG. 15

γ-ray energy spectrum observed when Monte Carlo generated ΛK^+K^- events can be fitted as $\Sigma^0 K^+K^-$

Ξ^* Mass resolution

FIG. 16

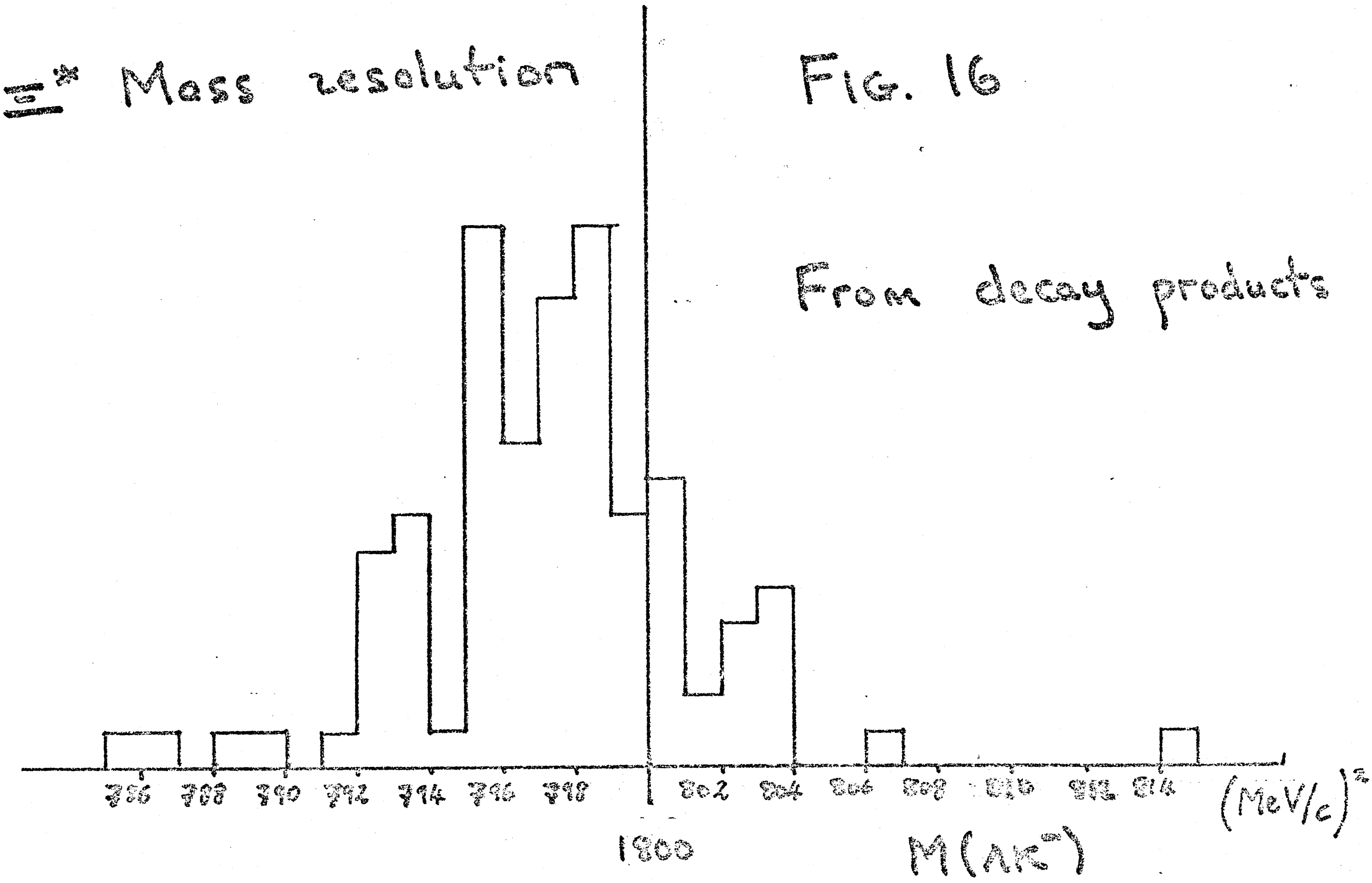

From decay products

After 4-C fit to $K^-p \to \Lambda K^+K^-$